A Novel Grid-Forming Strategy for Voltage-Source Controlled PV Under Nearly 100% Renewable Electricity

Pan Hu[1]*, Kezhen Jiang[1], Xiaotong Ji[2], Daojun Tan[1], Dan Liu[1], Kan Cao[1] and Wei Wang[2]

[1]*State Grid Hubei Electric Power Research Institute, Wuhan, China,* [2]*State Grid Hubei Electric Power Company Limited, Wuhan, China*
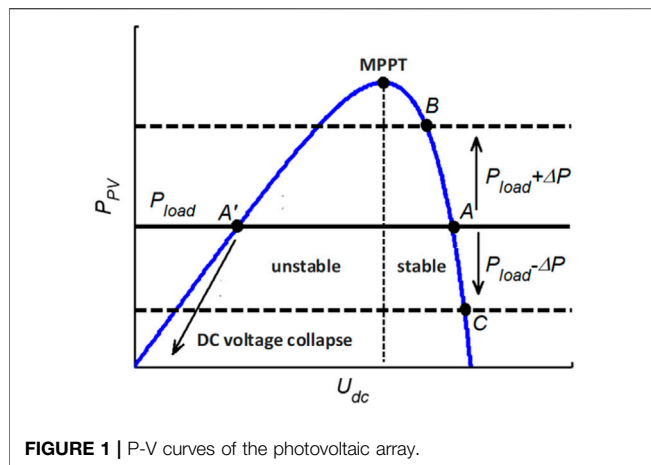
The demand for decarbonization calls for nearly 100% renewable electricity rising as the dominant power resource. The foregoing paradigm shifts require proactive voltage and frequency controllers for the converter-based renewable energy. This article proposed a novel grid-forming technique for voltage-source controlled photovoltaic (PV) operating in 100% renewable power systems. The proposed idea was to design a DC voltage collapse-prevention controller in conjunction with a simplified frequency and inertia controller, thereby smart capturing and releasing PV energy to achieve improvements in dynamic performance and efficiency. By setting the two-phase operation scheme, the model initiatively considers the conflict between frequency regulation and maximum power point tracking (MPPT) curve control. The preferred controls are validated using extensive simulation and experimental findings based on a semi-physical platform and a practical photovoltaic demonstration project. The proposed controller outperforms the standard PV current controller over a much larger range of weak grid situations, according to the experimental and engineering operational data. Results demonstrated the effectiveness of the presented method in applying to the future 100% renewable power system.

Keywords: grid-forming, voltage-source, controlled PV, 100% renewable electricity, DC voltage collapse-prevention controller

1 INTRODUCTION

Growing promises to reduce greenhouse gas emissions, as well as ambitious endeavors to minimize global average temperature rise, have driven efforts to decarbonize electricity, with a special emphasis on the use of renewable energy resources (Wu et al., 2021). The climate action plan necessitates the development of a nearly 100% renewable energy system and hence focuses on meeting the operation challenge of the uncertain nature of resources, primarily wind and solar PV. With RE becoming a prominent source in the system, the inverter-based or non-synchronous interface with the grid requires a proactive control strategy undertaking voltage and frequency regulation and support. Furthermore, grid-forming resources need to be widely used to improve synchronization stability in 100% renewable systems or weak grids (Blakers et al., 2019).

There, so far, mainly exists two types of inverter-based resources, i.e., the controlled current (CC) and the controlled voltage (CV) renewable sources (Fu et al., 2021). The CC type uses a phase-locked loop (PLL) to track the voltage and frequency at the point of common coupling (PCC) (Li et al., 2018; Zhou et al., 2018). Moreover, the CC interface often introduces voltage feed-forward (VFF) control to achieve improvement in dynamic response and harmonics suppression, which is particularly

FIGURE 1 | P-V curves of the photovoltaic array.

FIGURE 2 | DC voltage collapse-prevention controller.

appropriate for connecting to a strong grid. But at high penetration of RE, i.e., weak grid conditions, the CC controller also causes wide-frequency oscillation, causing harmonic resonance and system instability (Dong et al., 2015). With grid impedance fluctuation, the use of a VFF controller led to the positive feedback of grid impedance, resulting in injecting the harmonic current into weak grids and triggering a tendency toward progressive system instability. In addition, the PLL controller negatively affects the stability of CC inverters under weak grids. Xu et al. (2019) point out that the time delay in PLL brings a negative damping phenomenon, resulting in inverter oscillation. Meanwhile, in weak grids, the PLL bandwidth causes harmonic resonance. With the increase in bandwidth, the damping of the inverter impedance in the low-frequency band deteriorated (Silwal et al., 2019). Through the introduction of improved controllers, for example, time-delay compensation (Zhang et al., 2018), impedance reshaping (Fang et al., 2018a), and adaptive gain scheme (Xu et al., 2017), mitigates the preceding concerns; the dynamic performance of the CC interface is debased. In case of large transient disturbances, some CC renewable sources lose stable equilibrium points and synchronization stability (He et al., 2020). In light of the aforementioned drawbacks, CC resources are better suited for use in strong power systems.

For weak grids, especially under nearly 100% renewable electricity, the CV interface is proven to be a better solution than the CC interface. As a typical grid-forming resource, the CV types achieve power output directly by controlling the voltage vector phase and amplitude, enabling CV to be inherently synchronized with the grid without applying PLL (Yuan et al., 2009). CV resources proactively provide frequency and voltage modulation and moment of inertia if a virtual synchronous generator (VSG) is introduced (Zhong and Weiss, 2011). Furthermore, grid damping and impedance characteristics are increased without compromising CV interface dynamic performance under a lower short current ratio (SCR) (Wu et al., 2019). Therefore, the CV resources are thought to be an efficient solution and a significant component in the configuration of 100 percent renewable systems (Wang et al., 2020; Sang et al., 2022). To satisfy the CV interface requirement,
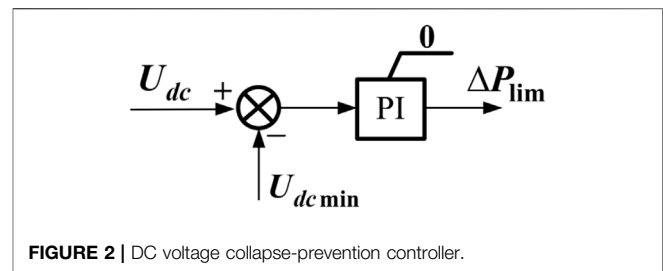
renewable resources typically add energy storage equipment into their DC side to counteract energy absorption or release in the dynamic regulation process, i.e., the unpredictability of wind and solar power (Liu et al., 2021). The energy storage handles the fast-varying power generated by inertia simulation through VSG control, whereas PV implements the portions of frequency regulation and adjusts for relatively long-term power variations with sluggish dynamics. As a result, the VSG provides a better dynamic frequency response during power fluctuations (Fang et al., 2018b; Debnath et al., 2021). To manage PV and energy storage resources, the integrated development combines enhanced control methods to offer inertial and main frequency response, reactive power support, and transient stability (Zhong and Weiss, 2011; Liu et al., 2021). However, virtual synchronous control often treats the DC side as the ideal source and ignores the energy storage limitation; it is difficult to apply it directly to RE's self-synchronous voltage source control. Moreover, because of the energy storage (ES), the traditional VSG technique is difficult to apply in a practical wind turbine and PV unit. ES increases the operation and maintenance workload after installation. The occupied space, geographical location, and machine requirements in the primary component of the original CC equipment restrict the application of ES and hence increase the potential challenges of CV sources used for wind turbines and PV (Imai et al., 2018). Therefore, a proposal for a grid-forming plan for each RE unit without the addition of energy storage is both promising and necessary. However, not much work deals with the above-mentioned relevant issues. This is mostly due to a clash between the uncertainty of RE output and the need for constant frequency support. The MPPT approach, for instance, is responsible for the output of PV arrays. The MPPT controller in the PV needs to be changed to set commands that absorb or release energy in accordance with the primary frequency control requirement. Therefore, the CV interface has the potential to cause PV DC voltage collapse, posing a threat to the PV safety and stability (Hua et al., 2017).

Inspiring by the aforementioned works, this article strived to carry out a novel grid-forming strategy for voltage-source controlled PV without adding energy storage. Thus, the proposed planning model provides a novel perspective of flexibility to operate with nearly 100% renewable electricity. The main contribution and novelty of our works settle in:

1) The article developed a DC voltage collapse-prevention controller that works in tandem with a simpler frequency

FIGURE 3 | Characteristic of multiple MPPT curves: **(A)** Typical P-V and I-V curves. **(B)** Multiple P-V curves of *PV*.

FIGURE 4 | Structure of the grid-forming controller with the DC voltage collapse-prevention controller. **(A)** Overall schematic controller of proposed CV-PV; **(B)** proposed frequency controller combined with DC voltage collapse-prevention controller.
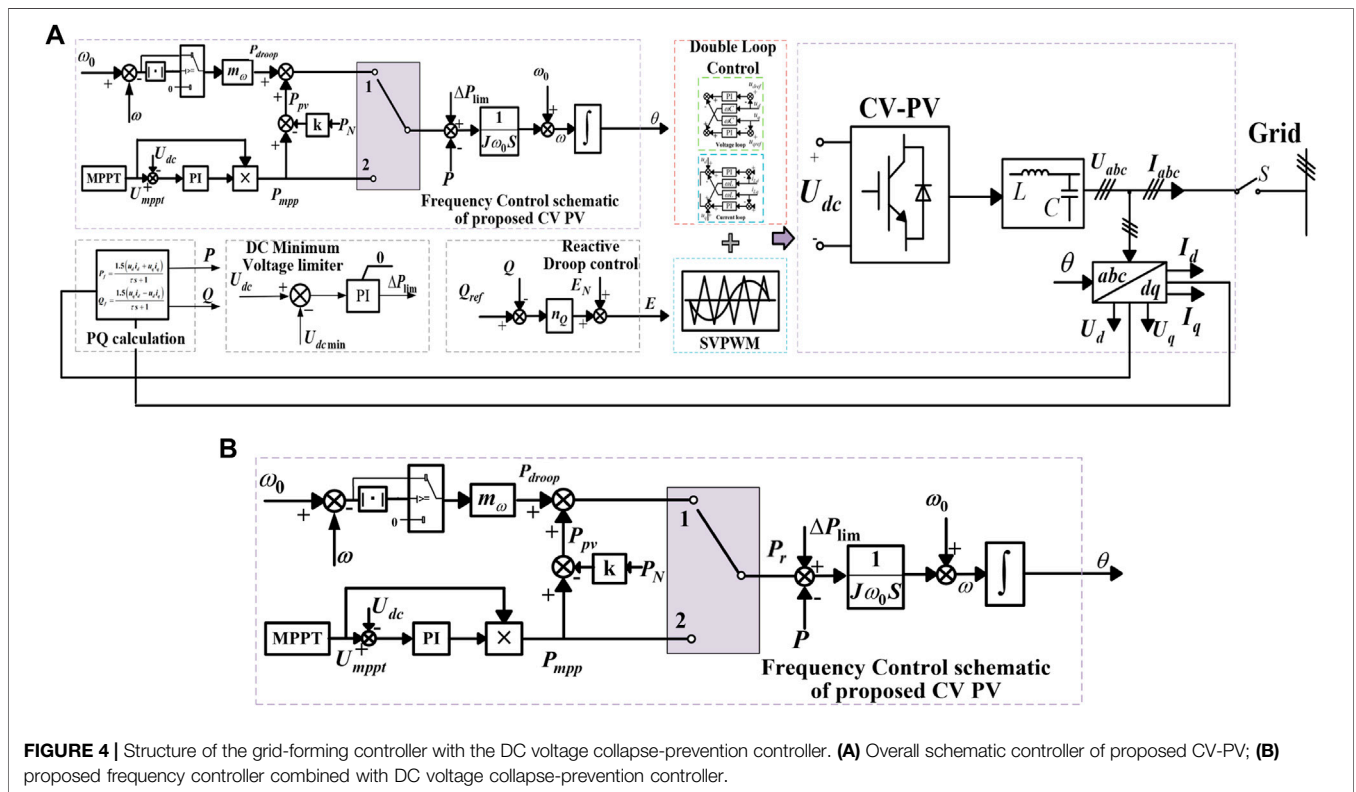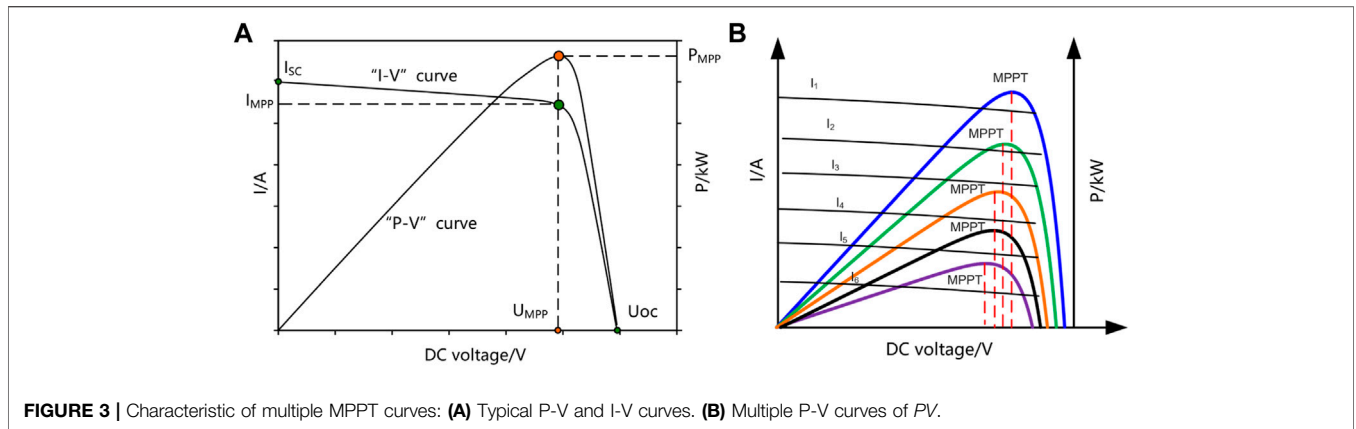
and inertia controller to capture and release PV energy intelligently. The model resolves the issue between frequency regulation and the MPPT approach by establishing the time accounting-storage strategy. The suggested control algorithm can offer adequate actual and reactive power services, as well as ensure PV DC voltage stability, under dynamic system operation and atmospheric circumstances, according to simulation findings obtained during system disruptions and rapid solar irradiation variations.

2) A CV interface and controller framework for the PV is proposed without including energy storage, combined with

the proposed model established by the DC voltage collapse-prevention controller and time accounting-storage method. By offering voltage and frequency control and supporting a weak grid, the unique grid-forming technique provides a perspective of flexibility to function in nearly 100% renewable electricity and an ability to design a weak grid.

The article is organized in the manner as follows. **Section 2** theoretically presents the main idea of DC voltage collapse prevention and gives the controller model. Subsequently, the CV interface and controller framework are put forward in **Section 3**. **Section 4** is devoted to the simulation and
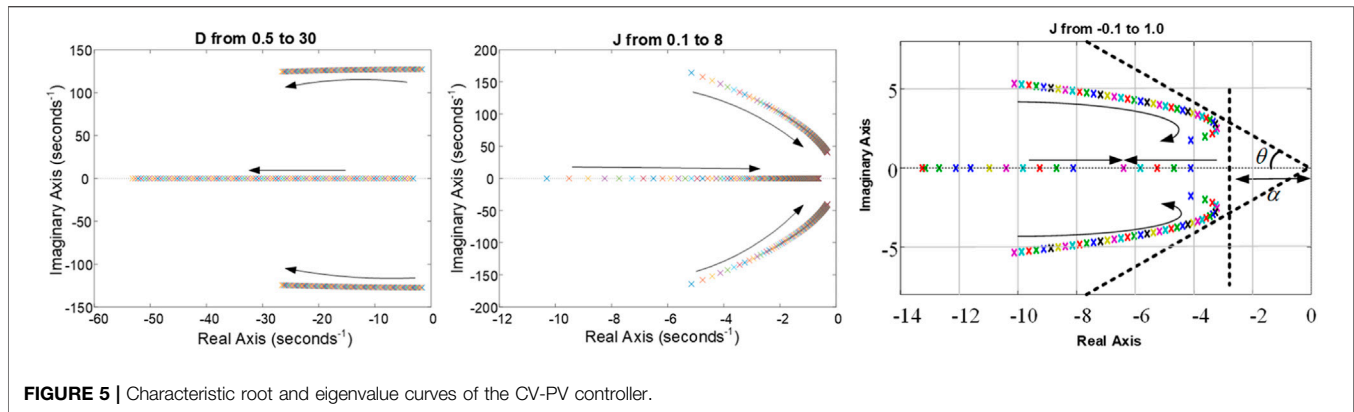
FIGURE 5 | Characteristic root and eigenvalue curves of the CV-PV controller.

hardware-in-the-loop (HIL) experiments and practical engineering verification. Conclusions and future works are summarized in **section 5**.

2 CONTROL STRATEGY AND SYSTEM DESIGN

2.1 Stable Operation Area of MPPT
To clearly analyze the stable operation area of MPPT and DC voltage stability, the following assumptions are put forward:

Assumption 1. The load is less than the PV array's maximum output power.

Assumption 2. The modulation ratio m of the PV inverter is sufficient.

As shown in **Figure 1**, the P-V curves indicate the following: 1) when U_{dc} is less than the MPPT DC voltage, the PV array's output P_{pv} grows as U_{dc} increases; 2) when U_{dc} is greater than the MPPT DC voltage, the P_{pv} declines as U_{dc} increases. Assuming P_{load} as the load power, U_{dc} corresponds to point A or A′ in **Figure 1**.

Due to voltage and frequency regulation requirements, if the load grows by ΔP while U_{dc} is at point A, the PV unit is required to produce additional energy to match the load. As a result, the extra power is provided by discharging the DC capacitor, and this results in a drop in U_{dc}. The drop in U_{dc} will cause P_{pv} to increase, according to the PV array's P-V characteristics. When P_{pv} equals $P_{load} + \Delta P$, U_{dc} shifts from point A to point B. U_{dc} is steady at operating point A, as can be shown. When the PV power supply is in this operating range, U_{dc} also exhibits a generator-like feature. When the load is increased or decreased, the DC voltage can be automatically discharged or charged, allowing the system to automatically undergo transition to the new balance point and maintain voltage and frequency stability without the need for further controls. When U_{dc} arrives at point A′, however, the situation is inverted. The DC capacitor discharges if the load increases by ΔP, and the fall of U_{dc} further reduces P_{pv} due to the PV array's P-V characteristics, exacerbating the imbalance between the PV output and the load r, eventually leading to the DC bus voltage collapse phenomenon. Furthermore, the inverter is considered to have a sufficient modulation ratio to

create the rated AC voltage in the preceding study. In practice, when U_{dc} falls below a particular threshold, m rises to 1. As U_{dc} falls, the AC output voltage falls as well, posing a major threat to the PV power supply system's safe and stable functioning. If the load is reduced by ΔP when U_{dc} is at point A′, the PV array charged the capacitor, increasing P_{pv} and accelerating the charging of the capacitor until U_{dc} passes the MPPT point and enters the stable region. The final operating point transits from point A′ to point C and lets the capacitor overvoltage. It is obvious that point A′ is the unstable operating point.

2.2 DC Voltage Collapse-Prevention Controller
Based on previous analysis, the DC voltage crosses the MPPT point into the unstable region, causing the DC bus voltage to collapse when the PV unit is overloaded. Affected by the variation in the luminous intensity, the maximum DC voltage and MPPT points vary simultaneously. The evolving MPPT curve makes determining the maximum P_{max} in time difficult, and if P_{max} exceeds the MPPT maximum power point, a DC voltage collapse occurs. If the DC voltage can be regulated directly during PV overload, it is envisaged that DC voltage collapse can be prevented.

The diagram of the DC voltage collapse-prevention controller is given in the **Figure 2** a follows:

The controller is a PI controller with an upper limit of 0. U_{dcmin} is the reference input signal, and ΔP_{lim} is the active power increment signal. The MPPT provides the U_{dcmin} command, which is the minimum MPPT voltage, as well as the minimum DC voltage at which the PV power supply can run at a steady state. The controller output is 0 when U_{dc} is greater than U_{dcmin}, and the PV operates in a droop state. Once U_{dc} falls below U_{dcmin}, this controller swiftly reduces the active power, bringing U_{dc} back to U_{dcmin}. ΔP_{lim} is presented as

$$\Delta \boldsymbol{P}_{lim} = \boldsymbol{k}_p \left(\boldsymbol{U}_{dc} - \boldsymbol{U}_{dcmin} \right) + \boldsymbol{k}_i \int \left(\boldsymbol{U}_{dc} - \boldsymbol{U}_{dcmin} \right) \mathbf{d}_t. \quad (1)$$

The principal frequency and inertia response can be met by reserving MPPT power, according to the aforementioned DC voltage collapse-prevention controller. However, due to the photoperiodic effect and the uncertainty of solar radiation, multiple MPPT curves exist, shown as in **Figure 3**. As a result,

TABLE 1 | Case scenario description.

Main electrocircuit parameter	Parameter value	Main electrocircuit parameter	Parameter value
AC rated voltage U_N/V	315	Rotational inertia	5
Maximum DC source voltage U_{dc}/V	1,000	Minimum DC source voltage U_{dc}/V	650
Filter inductor L/mH	18.4	Frequency droop coefficient	160
Filter capacitance C/μF	10	Voltage droop coefficient	0.01
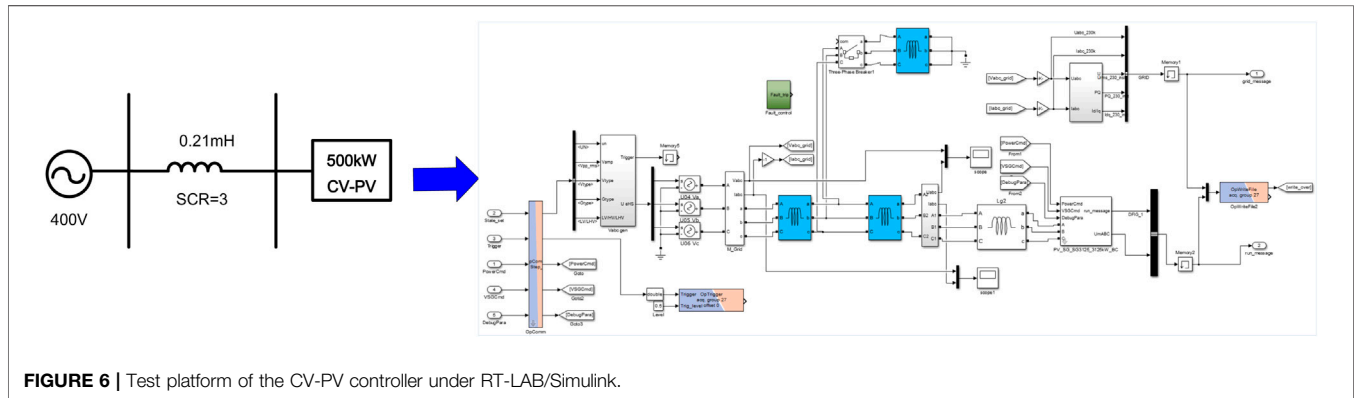
FIGURE 6 | Test platform of the CV-PV controller under RT-LAB/Simulink.

as solar radiation changes, the maximum power and lowest U_{dc} points fluctuate. This fact indicates that the DC voltage collapse-prevention controller has to set a bigger U_{dcmin} to prevent PV from running in the left area of P-V MPPT, resulting in more power loss. The constant DC voltage reduces the MPPT's operation margin, increasing the probability of a PV outage. To solve the aforementioned issue, a responding scheme is put forward.

This article designed a two-phase operation scheme for CV PV sources: the start-up phase and the frequency regulation phase.
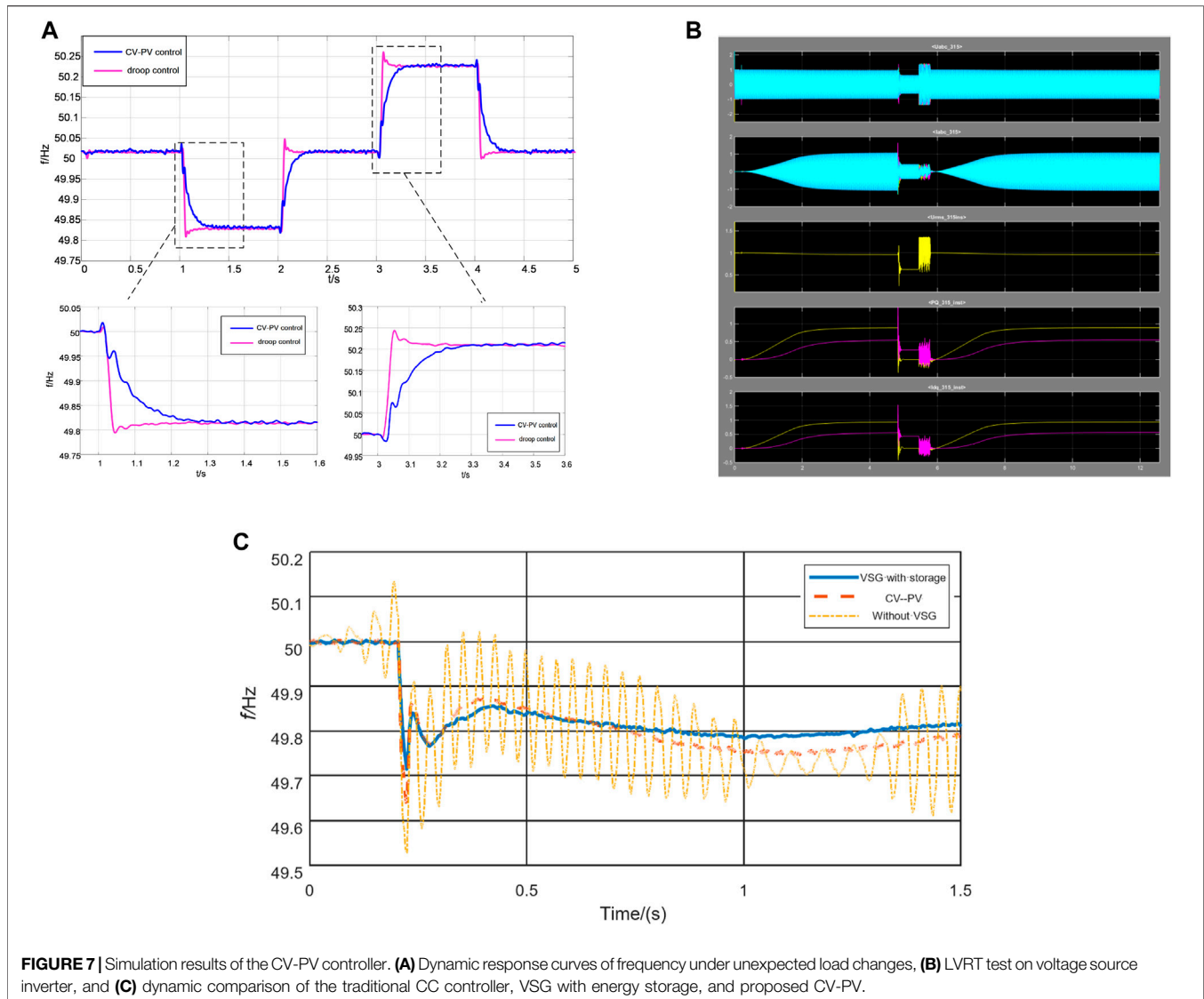
Start-up phase: After reaching the maximum power point, the controller enters the MPPT state first, starts the MPPT algorithm, and records the power and DC voltage.

Frequency regulation (FM) phase: The PV seamlessly switches from the MPPT state to FM state and closes the MPPT at the same time. After leaving the maximum power with a specified reserve k, i.e., generally 10 percent of the maximum PV power, the PV begins to participate in primary FM. The FM power is superimposed on the power command once it enters the steady state, and the output power is limited to the maximum PV power. PV uses the set modulation coefficient to calculate the primary FM power. The output active power is the sum of the specified power value after backup and the primary FM's steady-state power, shown in **Figure 4A**. When the FM power surpasses the reserved PV FM interval in the FM process, the PV operates at the maximum power of the MPPT point. The MPPT curve is refreshed every 500 ms. When MPPT point falls below 20% of the rated power, PV departs the FM mode.

2.3 Grid-forming Strategy for Voltage-Source Controlled PV

To clearly illustrate the main controller of the CV-PV, the overall schematic is shown in **Figure 4A**. Frequency and reactive controller, double loop and PWM module and power calculation, electrical measurement, and transformation module are the four basic components. The overall schematic controller takes advantage of the aforementioned technique paired with the proposed DC voltage collapse prevention by using a typical double closed-loop structure (Sun et al., 2021), P/f and Q/V droop management (Awal et al., 2020), and virtual rotor motion equations (Yuan et al., 2009). **Figure 4B** depicts the suggested frequency controller. A switcher in **Figure 4B** is designed to flexibly switch different frequency control modes. The P_{ref} in virtual rotor motion equations is the algebraic calculation of ΔP_{lim}, output active power P and P_r. When it switches to button 1, the CV-PV operates in the FM mode. In this mode, P_r is combined with P_{pv} and droop power P_{droop}. Moreover, P_{pv} is the sum of $k \times P_N$, i.e., power reservation of frequency regulation and MPPT power P_{mpp}. The incremental conductance algorithm (INC) (Liu et al., 2008) can be used to calculate the MPPT power P_{mpp} for a PV. The frequency and inertia-supporting ability of CV-PV is met in this FM mode by power reservation through $k \times P_N$. P_N is the rated power of CV-PV, and k is set to be 10%. To set an acceptable FM dead zone to prevent needless movement, the absolute value and comparison module are employed. To be noted, it causes electricity and energy loss during the FM mode, resulting in lowering the earnings of generation owners. Therefore, we put forward a switcher. When in button 2, P_r equals to P_{mpp}, i.e., close to the MPPT power. Furthermore, U_{mppt} is chosen to be 5–10 V bigger than the minimum DC voltage point from the MPPT curves, which is extremely close to the MPPT point, to improve the reliability of the proposed technique and provide an extra inertia energy source in this mode. The CV-PV does not engage in frequency control in this mode, but it does supply inertia and acts as a CV source to keep voltage and frequency stability in weak grids. The proposed schematic controller enhances the

FIGURE 7 | Simulation results of the CV-PV controller. **(A)** Dynamic response curves of frequency under unexpected load changes, **(B)** LVRT test on voltage source inverter, and **(C)** dynamic comparison of the traditional CC controller, VSG with energy storage, and proposed CV-PV.

economy of CV-PV. Moreover, in the transient process, the controller still employs the original CC low-voltage ride-through (LVRT) algorithm, i.e., the controller switches back to the CC mode during the fault period and changes back to CV control after the transient period is finished. Buraimoh et al. (2021) contains the transient controller strategy.

To test the proposed approach and calculate the PI and inertia parameters, Fu et al. (2021) introduced a small signal stability model. This is a summary of our earlier grid-forming controller work. The approach for detailed modeling can be found in the corresponding article. **Figure 5** shows the model's main parameters and the model findings, i.e., characteristic root and eigenvalue curves.

3 CASE STUDY AND ANALYSIS

Three scenarios, based on a semi-physical platform and a practical photovoltaic demonstration project, are used to

validate the suggested technique through comprehensive simulation and experimental data. The first example is an RT-LAB-based PV station simulation in Hubei, China. The purpose of this case was to analyze the controller's validity and dynamic characteristics for a PV station, as well as to optimize the parameters of these units under various circumstances. The PV station's hardware in-the-loop (HIL) tests with a CV-PV controller are then carried out in Case 2. As shown in the following figure, the EMT Hardware Solver (eHS) circuit of this PV is constructed in the RT-LAB platform, and the control component is accomplished by using a realistic DSP digital controller of SG500MX-V6, i.e., a 500 kW PV from Sungrow Company. The dynamic frequency response and voltage supporting findings are presented to illustrate the differences between the prior and optimal strategies for improving the PV's operation characteristics and resilience. The recording data and construction information of an actual PV engineering project are provided in Case 3. This project is the power side construction part of the 100% renewable energy
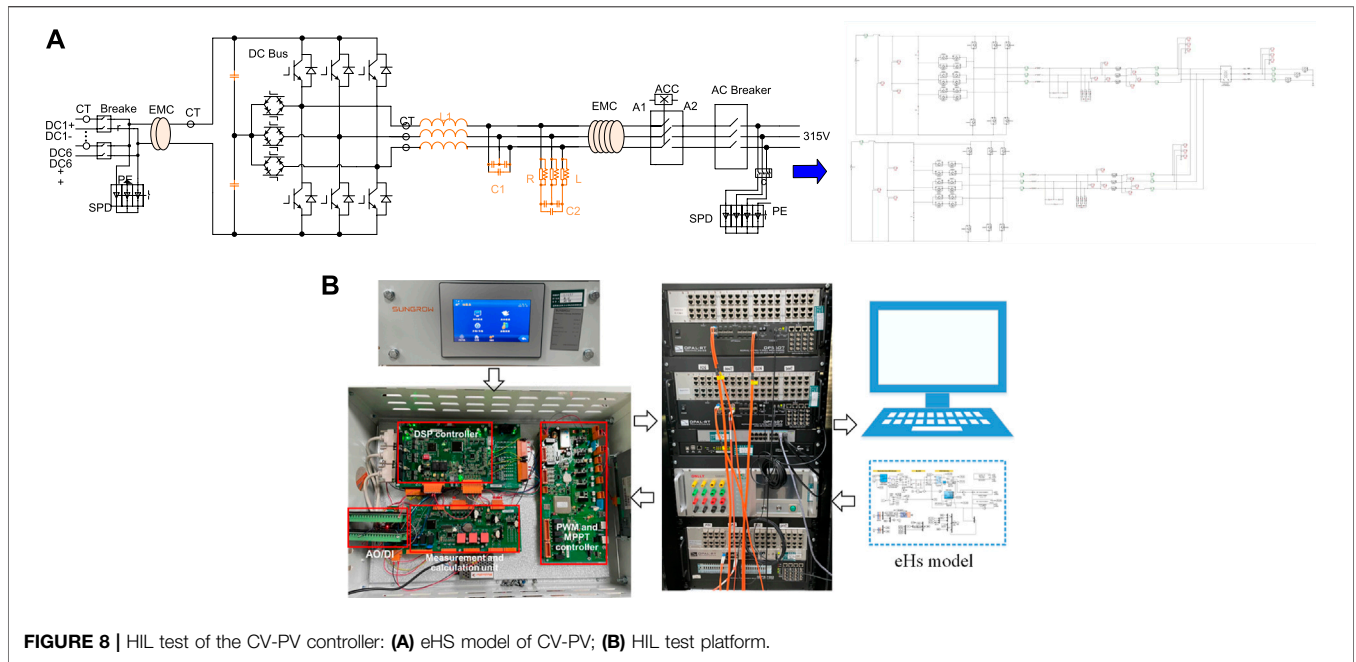
FIGURE 8 | HIL test of the CV-PV controller: **(A)** eHS model of CV-PV; **(B)** HIL test platform.

TABLE 2 | Case 2 scenario description.

No.	Test depicts	Scenario set and purpose
1	Active power control	From 0.1 to 0.8 p.u to test CV-PV control accuracy
2	MPPT control	MPPT test of power reserve response from 200 to 1000 rads
3	LVRT and HVRT test	Voltage from 1.0 to 0.3 p.u. and from 0.3 to 1.275 p.u.
4	Frequency droop test	Frequency varies from 50.5 to 49.5 Hz
5	Inertial test	Test power response when frequency varies within ±0.2 Hz

demonstration project in Suizhou, Hubei Province, China. About 32 MW PV will be updated and reformed to CV-PV. The findings of this study have already been implemented in engineering practice. The engineering data's detailed results demonstrated the practicality of the proposed solution in a large-scale renewable project. In all cases, the CV-PV controller's stability and dependability validated the proposed strategy.
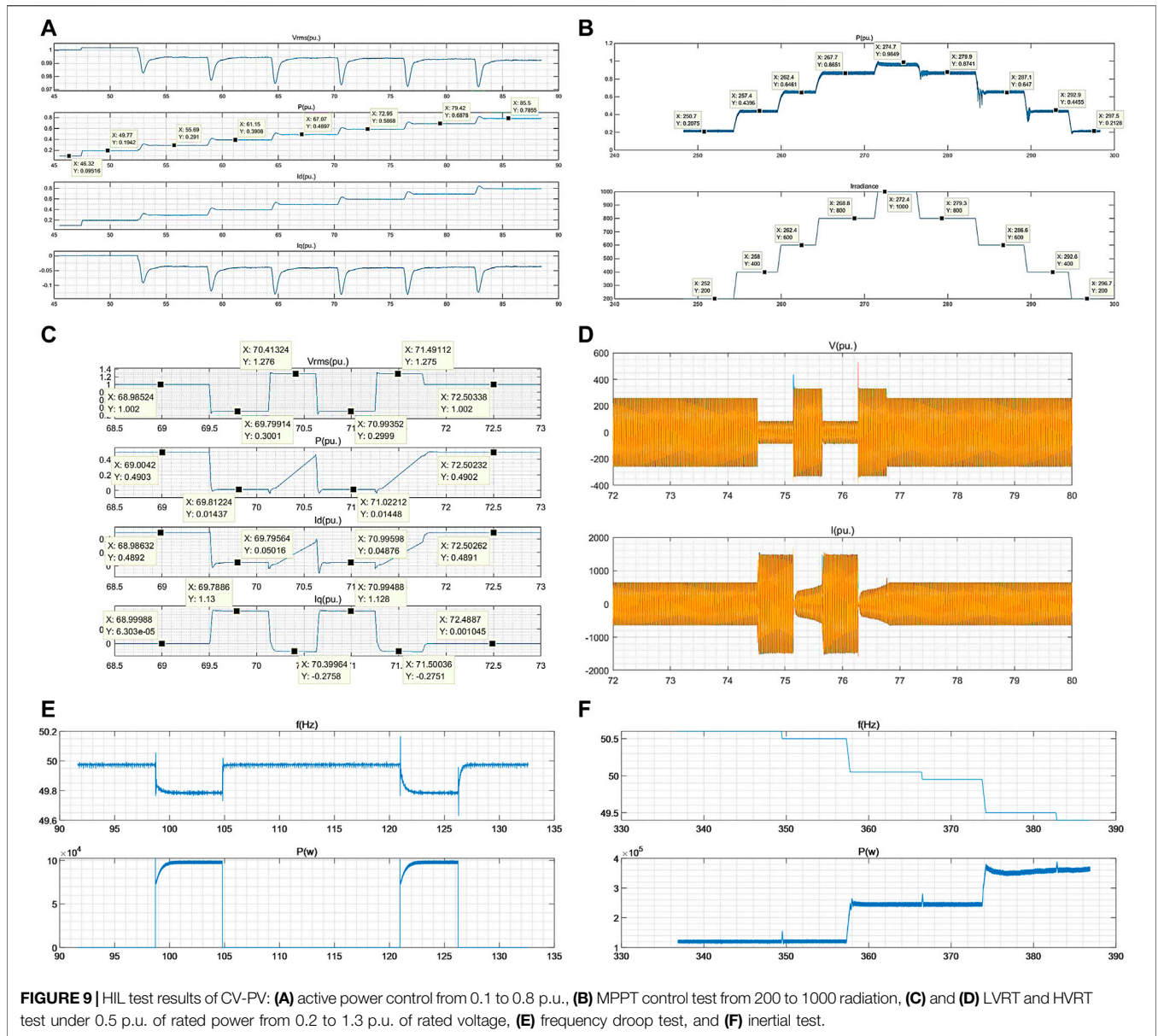
3.1 Case 1

An independent grid simulation model consisting of CV-PV is developed in RT-LAB/Simulink to verify the effectiveness of the controller technique, as shown in **Figure 6**. The parameters of this controller are given in the following **Table 1**. This test is a stand-alone system that consists of three parts: the grid part, the equivalent transmission line, and the tested equipment, of which

1) The grid part is built with the ideal voltage source model, and the power disturbance and fault ride-through configuration are completed by directly scaling the voltage source.
2) The analogous transmission line is designed inductively, with inductance used to represent the transformer and other

equipment in the transmission line above the equipment under test, and the short-circuit ratio is set to 1.5.
3) The proposed CV-PV inverter is used in the test equipment. Its dynamic characteristics of transient and steady response are used to determine the effectiveness of the control strategy.

The simulation timer is set to 5 sec. The initial local load is P_L = 400 kW and Q_L = 20 kVar; the load is increased to P_L = 420 kW and Q_L = 25 kVar at 1 s and returns to the initial value at 2 s; the load is reduced to P_L = 380 kW and Q_L = 10 kVar at 3 s and returns to the initial value at 4 s; the load is reduced to P_L = 380 kW and Q_L = 10 kVar at 3 s and returns. **Figure 7A** shows how the virtual proposed control approach compares to the traditional droop control strategy in terms of dynamic response curves of frequency under unexpected load changes. Low-voltage ride-through (LVRT) testing is performed on the voltage source inverter, in which the fault ride-through mimics balanced and unbalanced tests under 20% voltage dips. The inverter's steady-state working condition is set to 100% P_n for the duration of the test. **Figure 7B** shows the simulation results.

In **Figure 7C**, the comparison of the traditional CC controller, VSG with energy storage, and proposed CV-PV in frequency

FIGURE 9 | HIL test results of CV-PV: **(A)** active power control from 0.1 to 0.8 p.u., **(B)** MPPT control test from 200 to 1000 radiation, **(C)** and **(D)** LVRT and HVRT test under 0.5 p.u. of rated power from 0.2 to 1.3 p.u. of rated voltage, **(E)** frequency droop test, and **(F)** inertial test.

dynamic response is given. The setting of the simulation condition is the same as in Figure 7A, i.e., 20 kW active power disturbance is introduced. The results revealed that the proposed controller has a good behavior as traditional VSG with energy storage. As displayed in **Figure 7**, the system state does not lose stability in both power disturbance and transient periods. Obviously, the simulation results revealed that compared to the droop control, the control algorithm described in this research has a smoother frequency control impact, and its inertia features save time for future frequency regulation.

3.2 Case 2

In this scenario, HIL tests using grid-connected CV-PV are carried out. In **Figure 8A**, the controller circuit and the eHS model of the primary hardware element of the 500 kW PV are

shown, respectively. Two 500 kW PVs comprise a 1 MVA generation unit, as shown in **Figure 8A**, and power is transferred between them *via* a boosting transformer with split winding. The circulation current between CV-PV is generally limited due to the high impedance between split windings, especially when using the virtual impedance technique. The HIL experiments are carried out using this practical unit, and its platform is depicted in **Figure 8B**. The inverter control section of the DSP control board is primarily responsible for the output control signal. The metering board is primarily in charge of communicating with the touch screen. The transmission of trigger signals is handled by PWM and MPPT controllers. Operators can send power scheduling instructions, low penetration strategy coefficients, and key FM and inertia parameters using the parameter setting interface. To test the
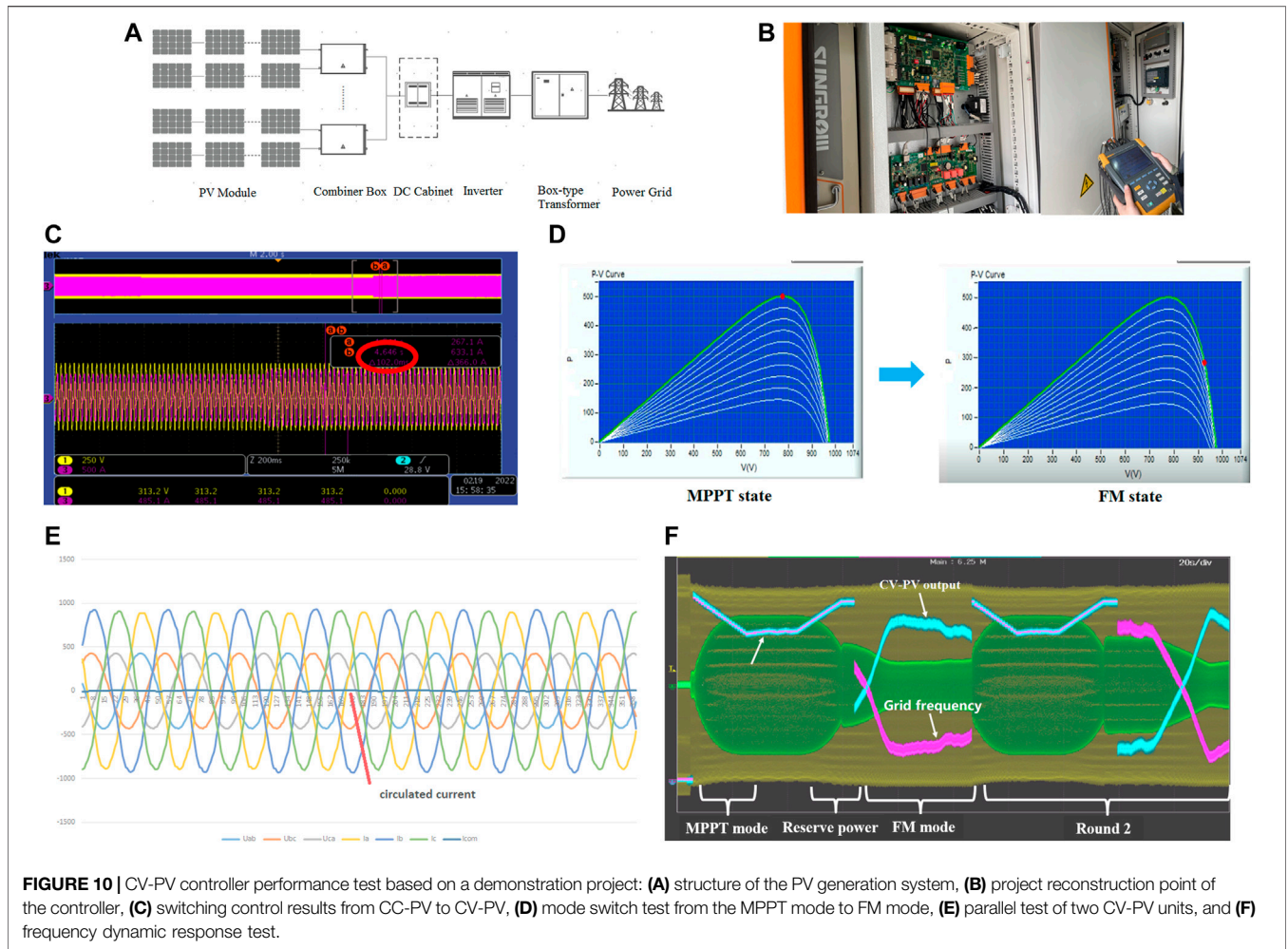
FIGURE 10 | CV-PV controller performance test based on a demonstration project: **(A)** structure of the PV generation system, **(B)** project reconstruction point of the controller, **(C)** switching control results from CC-PV to CV-PV, **(D)** mode switch test from the MPPT mode to FM mode, **(E)** parallel test of two CV-PV units, and **(F)** frequency dynamic response test.

dynamic response of this controller, a series of severity abnormal conditions are introduced and chosen to check the power disturbances and fault ride-through capabilities. The set of tests is depicted in **Table 2**, and the results are shown in **Figure 9**. Clearly, the experimental findings support the effectiveness of the controller's algorithm.

The active power of the CV-PV unit can be flexibly controlled, and the reaction time is less than 5 ms, indicating a quick control accuracy, as shown in **Figures 9A,B**. Based on the results in **Figures 9C,D**, the controller's transient behaviors are compatible with the original CC-PV (d). Moreover, in **Figures 10E,F**, the simulation results clearly illustrate that the frequency and inertia characteristics have an influence on the controller's output. The HIL test verifies the proposed controller's validity and benefits.

3.3 Case 3

A demonstration project is introduced here to verify the validity of the grid-forming strategy. The hybrid renewable station which consists of wind and solar energy is located in the middle of Hubei province, China. The capacity of permanent magnet direct-drive wind is 41.6 MW, while the rated photovoltaic is about 50 MW. Considering the economic and construction aspects, about 60%

of PV units are upgraded as voltage-source by utilizing the same CV-PV controller in Case 2. The technical transformation enables the CV-PV to achieve the following functions, especially including the droop and inertia control mode, PQ control mode, seamless switching between them, and provision of reactive voltage support.

Several frequency disturbances are exerted on the secondary windings of the current transformer. The PV responses and its inner MPPT control results are shown in **Figure 10**. For instance, the switching time in **Figure 10C** is approximately 102 ms, and the circulation current between two CV-PV is nearly 0. In **Figure 10F**, the frequency response and its inner power reservation results are present. According to the process of dynamic response, the effectiveness and correctness of the proposed algorithm in a real engineering project are tested.

4 CONCLUSION

This work introduced a unique grid-forming CV-PV controller that can be used to establish a nearly 100% renewable electricity system without the need for energy storage on the DC side. Under dynamic system operation and atmospheric conditions, the

proposed control algorithm provides acceptable actual and reactive power services, as well as PV DC voltage stability. Based on a semi-physical platform and a practical photovoltaic demonstration project, the major conclusions include the following:

1) To intelligently capture and release PV energy, the study built a DC voltage collapse-prevention controller that worked in combination with a simpler frequency and inertia controller. The experimental findings based on a semi-physical platform and a realistic DSP digital controller confirmed that the controller has high dynamic performance and stability.
2) With the suggested model built by the time accounting-storage approach, the CV interface and controller framework for PVs are proposed without integrating energy storage. The model anticipated the conflict between frequency regulation and curve control using the MPPT. The outcomes of the demonstration project attested to the method's efficacy.

Admittedly, concerning the proposed planning model, a few aspects can be enriched, such as the reduction of reserved power and the consideration of the supportability of transient reactive power.

REFERENCES

Awal, M. A., Yu, H., Lukic, S., and Husain, I. (2020). Droop and Oscillator Based Grid-Forming Converter Controls: A Comparative Performance Analysis. *Front. Energy Res.* 8, 3–6. doi:10.3389/fenrg.2020.00168

Blakers, A., Stocks, M., Lu, B., Cheng, C., and Stocks, R. (2019). Pathway to 100% Renewable Electricity. *IEEE J. Photovoltaics* 9 (6), 1828–1833. doi:10.1109/JPHOTOV.2019.2938882

Buraimoh, E., Davidson, I. E., and Martinez-Rodrigo, F. (2021). Decentralized Fast Delayed Signal Cancelation Secondary Control for Low Voltage Ride-Through Application in Grid Supporting Grid Feeding Microgrid. *Front. Energy Res.* 9, 4–8. doi:10.3389/fenrg.2021.643920

Debnath, S., Marthi, P. R. V., Xia, Q., Pan, J., Saeedifard, M., Vipin, V. N., et al. (2021). Renewable Integration in Hybrid AC/DC Systems Using a Multi-Port Autonomous Reconfigurable Solar Power Plant (MARS). *IEEE Trans. Power Syst.* 36 (1), 603–612. Jan. 2021. doi:10.1109/TPWRS.2020.3037520

Dong, D., Wen, B., Boroyevich, D., Mattavelli, P., and Xue, Y. (2015). Analysis of Phase-Locked Loop Low-Frequency Stability in Three-phase Grid-Connected Power Converters Considering Impedance Interactions. *IEEE Trans. Ind. Electron.* 62 (1), 310–321. doi:10.1109/tie.2014.2334665

Fang, J., Li, X., Li, H., and Tang, Y. (2018a). Stability Improvement for Three-phase Grid-Connected Converters through Impedance Reshaping in Quadrature-Axis. *IEEE Trans. Power Electron.* 33 (10), 8365–8375. doi:10.1109/tpel.2017.2777972

Fang, J., Tang, Y., Li, H., and Li, X. (2018b). A Battery/Ultracapacitor Hybrid Energy Storage System for Implementing the Power Management of Virtual Synchronous Generators. *IEEE Trans. Power Electron.* 33 (4), 2820–2824. doi:10.1109/TPEL.2017.2759256

Liu, F., Duan, S., Liu, F., Kang, B., and Kang, Y. (2008). A Variable Step Size INC MPPT Method for PV Systems. *IEEE Trans. Ind. Electron.* 55 (7), 2622–2628. doi:10.1109/TIE.2008.920550

Fu, X., Sun, J., Huang, M., Tian, Z., Yan, H., Iu, H. H.-C., et al. (2021). Large-Signal Stability of Grid-Forming and Grid-Following Controls in Voltage Source Converter: A Comparative Study. *IEEE Trans. Power Electron.* 36 (7), 7832–7840. doi:10.1109/TPEL.2020.3047480

He, X., Geng, H., Li, R., and Pal, B. C. (2020). Transient Stability Analysis and Enhancement of Renewable Energy Conversion System during LVRT. *IEEE Trans. Sustain. Energy* 11 (3), 1612–1623. doi:10.1109/tste.2019.2932613

Hua, T., Yan, X., and Fan, W. (2017). "Research on Power Point Tracking Algorithm Considered Spinning Reserve Capacity in Gird-Connected Photovoltaic System Based on VSG Control Strategy," in *IEEE 3rd International Future Energy Electronics Conference and ECCE Asia (IFEEC 2017 - ECCE Asia)*, 2059–2063. doi:10.1109/IFEEC.2017.7992368

Imai, H., Orihara, D., Iioka, D., and Saitoh, H. (2018). A Novel Virtual Synchronous Generator Control of PMSG-Based Wind Generation System to Enhance Transient Stability of Power System," in *IEEE Electronic Power Grid eGrid*, 1–6. doi:10.1109/eGRID.2018.8598690

Li, M., Zhang, X., and Zhao, W. (2018). A Novel Stability Improvement Strategy for a Multi-Inverter System in a Weak Grid Utilizing Dual-Mode Control. *Energies* 11 (8), 2144. doi:10.3390/en11082144

Liu, J., Golpira, H., Bevrani, H., and Ise, T. (2021). Grid Integration Evaluation of Virtual Synchronous Generators Using a Disturbance-Oriented Unified Modeling Approach. *IEEE Trans. Power Syst.* 36 (5), 4660–4671. doi:10.1109/tpwrs.2021.3061615

Sang, S., Zhang, C., Zhang, J., Shi, G, and Deng, F (2022). Analysis and Stabilization Control of a Voltage Source Controlled Wind Farm under Weak Grid Conditions. *Front. Energy* 2095–1698, 3–8. doi:10.1007/s11708-021-0793-5

Silwal, S., Taghizadeh, S., Karimi-Ghartemani, M., Hossain, M. J., and Davari, M. (2019). An Enhanced Control System for Single-phase Inverters Interfaced with Weak and Distorted Grids. *IEEE Trans. Power Electron.* 34 (12), 12538–12551. doi:10.1109/tpel.2019.2909532

Sun, Z., Zhu, F., and Cao, X. (2021). Study on a Frequency Fluctuation Attenuation Method for the Parallel Multi-VSG System. *Front. Energy Res.* 9 , 4–6. doi:10.3389/fenrg.2021.693878

Wang, X., Taul, M. G., Wu, H., Liao, Y., Blaabjerg, F., and Harnefors, L. (2020). Grid-Synchronization Stability of Converter-Based Resources-An Overview. *IEEE Open J. Ind. Appl.* 1, 115–134. doi:10.1109/ojia.2020.3020392

Wu, C., Zhang, X. -P., and Sterling, M. J. H. (2021). Global Electricity Interconnection with 100% Renewable Energy Generation. *IEEE Access* 9, 113169–113186. doi:10.1109/ACCESS.2021.3104167

Wu, W., Zhou, L., Chen, Y., Luo, A., Dong, Y., Zhou, X., et al. (2019). Sequence-Impedance-Based Stability Comparison between VSGs and Traditional Grid-

DATA AVAILABILITY STATEMENT

The original contributions presented in the study are included in the article/Supplementary Material; further inquiries can be directed to the corresponding author.

AUTHOR CONTRIBUTIONS

PH selected and studied the sources, designed the structure of the manuscript, and wrote the first draft of the manuscript. KJ and XJ contributed with supervision over the study of the literature and the writing of the manuscript. KC and DL modified the topology of this manuscript. DT designed the HIL test platform. All authors contributed to manuscript revision, read, and approved the submitted version.

FUNDING

Connected Inverters. *IEEE Trans. Power Electron.* 34 (1), 46–52. doi:10.1109/tpel.2018.2841371

Yuan, X. B., Wang, F., Boroyevich, D., Yongdong, L., and Burgos, R. (2009). DC-link Voltage Control of a Full Power Converter for Wind Generator Operating in Weak-Grid Systems. *IEEE Trans. Power Electron.* 24 (9), 2178–2192. doi:10.1109/tpel.2009.2022082

Xu, J., Qian, Q., Zhang, B., and Xie, S. (2019). Harmonics and Stability Analysis of Single-phase Grid-Connected Inverters in Distributed Power Generation Systems Considering Phase-Locked Loop Impact. *IEEE Trans. Sustain. Energy* 10 (3), 1470–1480. doi:10.1109/tste.2019.2893679

Xu, J., Xie, S., Qian, Q., and Zhang, B. (2017). Adaptive Feedforward Algorithm without Grid Impedance Estimation for Inverters to Suppress Grid Current Instabilities and Harmonics Due to Grid Impedance and Grid Voltage Distortion. *IEEE Trans. Ind. Electron.* 64 (9), 7574–7586. doi:10.1109/tie.2017.2711523

Zhang, X., Xia, D., Fu, Z., Wang, G., and Xu, D. (2018). An Improved Feedforward Control Method Considering PLL Dynamics to Improve Weak Grid Stability of Grid-Connected Inverters. *IEEE Trans. Ind. Appl.* 54 (5), 5143–5151. doi:10.1109/tia.2018.2811718

Zhong, Q.-C., and Weiss, G. (2011). Synchronverters: Inverters that Mimic Synchronous Generators. *IEEE Trans. Ind. Electron.* 58 (4), 1259–1267. doi:10.1109/tie.2010.2048839

Zhou, S., Zou, X., Zhu, D., Tong, L., Zhao, Y., Kang, Y., et al. (2018). An Improved Design of Current Controller for LCL-type Grid-Connected Converter to Reduce Negative Effect of PLL in Weak Grid. *IEEE J. Emerg. Sel. Top. Power Electron.* 6 (2), 648–663. doi:10.1109/jestpe.2017.2780918

Conflict of Interest: Authors PH, KJ, XJ, DT, DL, KC and WW were employed by State Grid Hubei Electric Power Company Limited.

Publisher's Note: All claims expressed in this article are solely those of the authors and do not necessarily represent those of their affiliated organizations, or those of the publisher, the editors, and the reviewers. Any product that may be evaluated in this article, or claim that may be made by its manufacturer, is not guaranteed or endorsed by the publisher.